Biophysical and Biological Studies of End-Group-Modified Derivatives of Pep-1[†]

K. Weller,[‡] S. Lauber,[§] M. Lerch,[§,||] A. Renaud,[⊥] H. P. Merkle,[‡] and O. Zerbe*,[⊥]

Drug Formulation and Delivery Group, Department of Chemistry and Applied BioSciences, ETH Zurich, Wolfgang-Pauli-Strasse 10, CH-8093 Zurich, Switzerland, Department of Chemistry and Applied BioSciences, ETH Zurich, CH-8093 Zurich, Switzerland, and Institute of Organic Chemistry, University of Zurich, Winterthurerstrasse 190, CH-8057 Zurich, Switzerland

Received August 2, 2005; Revised Manuscript Received October 11, 2005

ABSTRACT: Pep-1 is a tryptophane-rich cell-penetrating peptide (CPP) that has been previously proposed to bind protein cargoes by hydrophobic assembly and translocate them across cellular membranes. To date, however, the molecular mechanisms responsible for cargo binding and translocation have not been clearly identified. This study was conducted to gain insight into the interaction between Pep-1 with its cargo and the biological membrane to identify the thereby involved structural elements crucial for translocation. We studied three peptides differing in their N- and C-termini: (i) Pep-1, carrying an acetylated N-terminus and a C-terminal cysteamine elongation, (ii) AcPepWAmide, with an acetylated N-terminus and an amidated C-terminus, and (iii) PepW, with two free termini. Thioredoxin (TRX) and β-galactosidase were used as protein cargoes. To study CPP−membrane interactions, we performed biophysical as well as biological assays. To mimic biological membranes, we used phospholipid liposomes in a dye leakage assay and surfactant micelles for high-resolution NMR studies. In addition, membrane integrity, cell viability, and translocation efficiency were analyzed in HeLa cells. An α-helical structure was found for all peptides in the hydrophobic N-terminal region encompassing residues 4−13, whereas the hydrophilic region remained unstructured in the presence of micelles. Our results show that the investigated peptides interacted with the micelles as well as with the protein cargo via their tryptophan-rich domain. All peptides displayed an orientation parallel to the micelle surface. The C-terminal cysteamine group formed an additional membrane anchor, leading to more efficient translocation properties in cells. No membrane permeabilization was observed, and our data were largely compatible with an endocytic pathway for cellular uptake.

Chemical or physical linkage to so-called cell-penetrating peptides (CPPs)[1] is a widely studied approach to enable the cellular translocation of biomacromolecules, such as peptides, proteins, and nucleic acids, that otherwise cannot pass through cellular membranes. Therefore, the interactions between CPP and the cell membrane, as well as the underlying mechanisms for translocation, have been a preferred subject in CPP research, but are yet far from being understood in full detail. Much attention has been attracted by the structural prerequisites that are necessary for the cellular translocation of CPP (*1*, *2*). Typically, most studies that aim to identify the underlying mechanism focus on either a cell biological or a biophysical type of approach. Studies that combine biophysical and cell biological approaches are rare (*2*, *3*).

The mechanistic conclusions that were proposed in the field have been diverse (*4*). With respect to an energy-independent type of translocation, three different models have been recently reviewed by Lundberg et al. (*5*): the inverted micelle, the barrel stave, and the carpet/torroidal pore hypotheses. On the other hand, interactions between CPP and the cell membrane were proposed to trigger energy-dependent pathways, i.e., endocytosis. A growing body of experimental evidence for this pathway has recently accumulated (*6*, *7*).

Previously, a synthetic CPP, coined Pep-1, also known as the Chariot peptide (Instruction manual, Chariot, Active Motif Europe, Rixensart, Belgium), has been introduced as a vector that binds protein cargoes in a noncovalent fashion (*4*, *8*−*10*). The peptide contains an N-terminal, nonpolar tryptophan-rich domain, and a C-terminal oligocationic nuclear localization sequence (NLS) derived from the simian

[†] This work was supported by the Commission of the European Union (EU project on Quality of life and Management of Living Resources, Project QLK2-CT-2001-01451).

* To whom correspondence should be addressed: Institute of Organic Chemistry, University of Zurich, Winterthurerstr. 190, CH-8057 Zurich, Switzerland. Phone: +41 44 635 42 63. Fax: +41 44 635 68 33. E-mail: oliver.zerbe@oci.unizh.ch.

[‡] Drug Formulation and Delivery Group, Department of Chemistry and Applied BioSciences, ETH Zurich.

[§] Department of Chemistry and Applied BioSciences, ETH Zurich.

[||] Present address: Department of Biochemistry and Biophysics, Stockholm University, Stockholm, Sweden.

[⊥] University of Zurich.

[1] Abbreviations: CLSM, confocal laser scanning microscopy; CPP, cell-penetrating peptide; DPC, d_{38}-dodecylphosphocholine; FACS, fluorescence-activated cell sorting; FCS, fetal calf serum; HBSS, Hank's Balanced Salt Solution; MOPS, 3-(*N*-morpholino)propanesulfonic acid; MTT, 3-(4,5-dimethylthiazol-2-yl)-2,5-diphenyltetrazolium bromide; PI, propidium iodide; POPC, 1-palmitoyl-2-oleoyl-*sn*-glycero-3-phosphocholine; POPG, 1-palmitoyl-2-oleoyl-*sn*-glycero-3-[phospho-*rac*-(1-glycerol)] sodium salt; SDS, d_{25}-sodium dodecyl sulfate; TRX, thioredoxin.

10.1021/bi051535d CCC: $30.25
Published on Web 11/10/2005

virus 40 large T antigen. The two elements are connected through the self-fluorescent WSQP spacer, resulting in an amphiphilic sequence (*8*).

It has been proposed that Pep-1 associates with its protein cargo via its tryptophan-rich motif (*4*, *8*). Deshayes et al. postulated that the cellular translocation of Pep-1 involves the transient assembly of the peptide in the membrane such that pores are formed. Their model was directly derived from the results of biophysical studies, in combination with electrophysiological recordings with oocytes. In contrast, Henriques et al. found no evidence for pores or other lytic structures using photophysical techniques (*9*). Herein, we present a study with a set of peptides differing in their N- and C-termini: (i) Pep-1, which contains an acetylated N-terminus and a C-terminal cysteamine extension, (ii) AcPepWAmide, with an acetylated N-terminus and an amidated C-terminus, and (iii) PepW, with free N- and C-termini.

We conducted biophysical experiments to analyze peptide−membrane interactions using a liposome leakage assay and studied peptide−cargo interactions by NMR, applying a chemical shift mapping methodology with thioredoxin (TRX) serving as a cargo. Moreover, we determined the structures of the peptides by NMR in the presence of 90% d_{38}-dodecylphosphocholine (DPC)/10% d_{25}-sodium dodecyl sulfate (SDS) micelles. The topology of the peptide−membrane interface was probed by NMR with the spin-label 5-doxylstearate. Finally, the potency of the peptides for membrane translocation was investigated in HeLa cells with fluorescein-labeled TRX or β-galatosidase as the cargo. We also measured membrane integrity and cell viability in this cell line.

For all three peptides, the N-terminal region folds into an amphipathic helix in the presence of the phospholipid micelles whereas the hydrophilic C-terminal region remains unstructured. The Trp residues serve as the main membrane-anchoring residues causing the peptide to be parallel to the membrane surface. Interactions between the peptides and TRX exclusively involved hydrophobic surface residues of the latter. By comparing the membrane binding properties of the three CPPs, we observed that membrane anchoring of the peptide was more efficient in the presence of the C-terminal cysteamine group, accompanied by more efficient translocation properties in our cellular uptake studies. Finally, the experimental data of this work indicate that the observed peptide−membrane interactions might serve as a first step toward endocytic translocation.

MATERIALS AND METHODS

Materials. Deuterated dodecylphosphatidylcholine (DPC-d_{38}, 99% D), d_{25}-sodium dodecyl sulfate (SDS), and dideuterium oxide (D_2O) were ordered from Cambridge Isotope Laboratories (Andover, MA). 1-Palmitoyl-2-oleoyl-*sn*-glycero-3-phosphocholine (POPC) and 1-palmitoyl-2-oleoyl-*sn*-glycero-3-[phospho-*rac*-(1-glycerol)] sodium salt (POPG), both of the best quality available, were purchased from Avanti Polar Lipids (Alabaster, AL) and used without further purification. Melittin (>93% pure) and 5-doxylstearic acid were received from Aldrich (Buchs, Switzerland), and Calcein and phosphate-buffered saline (PBS) for buffer preparation as well as a 0.4% Trypan Blue solution in 0.81% sodium chloride and 0.06% potassium phosphate were purchased from Fluka (Buchs, Switzerland). HeLa cells were obtained from American Type Culture Collection (ATCC, Rockville, MD). Cell culture media, trypsin-EDTA, penicillin, streptomycin, and Hank's Balanced Salt Solution (HBSS) were bought from Gibco (Paisley, U.K.). Fetal calf serum (FCS) was obtained from Fisher Scientific (Wohlen, Switzerland). Hoechst 33342 and propidium iodide (PI) were from Molecular Probes (Leiden, The Netherlands), and 3-(4,5-dimethylthiazol-2-yl)-2,5-diphenyltetrazolium bromide (MTT) from Sigma (St. Louis, MO). Pep-1 (also denoted Chariot) is a component of the Chariot transfection reagent, also containing β-galactosidase. The Chariot transfection reagent and the related β-galactosidase staining kit were purchased from Activemotife (Carlsbad, CA), and fluorescein 5-maleimide was from Molecular Probes (Eugene, OR).

Table 1: Amino Acid Sequences and Molecular Masses of the Examined CPPs

name	sequence	molecular mass[a] (Da)
Pep-1	Ac-KETWWETWWTEWSQPKKKRK-Cya	2948.5
AcPepWAmide	Ac-KETWWETWWTEWSQPKKKRK-amide	2886.5
PepW	KETWWETWWTEWSQPKKKRK	2845.5

[a] Calculated molecular mass of the CPP.

CPP. The amino acid sequences of all investigated CPP are listed in Table 1. The structural elements of the CPP are a N-terminal nonpolar tryptophan-rich motif and the C-terminal oligocationic sequence of simian virus (SV) 40 large T antigen, also known as a nuclear localization sequence (NLS), conjugated via the self-fluorescent WSQP spacer (*8*). Pep-1 was synthesized by NMI TT GmbH (Reutlingen, Germany) and used without further purification. AcPepWAmide and PepW were synthesized on an ABI 433A peptide synthesizer (Applied Biosystems) by means of standard solid-phase Fmoc chemistry. AcPepWAmide and PepW were assembled on Rink amide resin MBHA and on 2-chlorotrityl resin, respectively, preloaded with Fmoc-Lys(Boc)-OH. At the end of the synthesis, the N-terminus of AcPepWAmide was acetylated on the resin using the capping procedure of the manufacturer. After cleavage from the resin and removal of the side chain protecting groups using a TFA/H_2O/TIS mixture (95:2.5:2.5), AcPepWAmide and PepW were purified by preparative RP-HPLC and identified by MALDI-TOF-MS: PepW, calculated mass 2845.5, measured mass ($[M + H]^+$) 2847.6; AcPepWAmide, calculated mass 2886.5, measured mass ($[M + H]^+$) 2889.7. The purity of all CPP was analyzed using HPLC and MALDI-MS, and was found to be >96%.

Preparation of ^{15}N-Labeled TRX. The pET14b plasmid containing the cDNA of N-terminal hexa-His-tagged TRX with a downstream enterokinase cleavage site was kindly provided by the group of J. Robinson (Institute of Organic Chemistry, University of Zurich). The cleavage site was replaced by a regular stop codon using site-directed mutagensis, and the sequence was confirmed by dideoxy sequencing. The ^{15}N-labeled protein was expressed in *Escherichia coli* strain BL21(DE3)pLysS at 37 °C on minimal M9 medium containing $[^{15}N]NH_4Cl$ as the sole nitrogen source. After cell lysis and separation of the cell debris by centrifugation, the supernatant was applied to a Ni affinity column and eluted with 100 mM imidazole. Protein-

containing fractions were desalted and subsequently lyophilized. Expression and purification were controlled by SDS−PAGE, and the labeled protein was finally characterized by ESI-MS. Moreover, sample integrity and purity were checked by recording an $^{15}N-^{1}H$ HSQC NMR spectrum, and peak positions therein were compared to published data (*11*).

NMR Spectroscopy. All NMR experiments were performed with 2 mM solutions of the corresponding CPP at pH 5.6 in the presence of 270 mM d_{38}-dodecylphosphocholine (DPC) and 30 mM d_{25}-sodium dodecyl sulfate (SDS) in a 90% H_2O/10% D_2O mixture (*12*). We co-added 10 mol % SDS to mimic the partial negative charge of biological membranes. Spectra were recorded at 310 K on a Bruker DRX-500 spectrometer. Sequence-specific resonance assignments were performed using a methodology developed by Wüthrich and co-workers (*13*) based on 12 and 40 ms clean TOCSY experiments (*14*) and on a 120 ms NOESY experiment (*15*), which was modified to incorporate a filter for suppression of zero-quantum coherences (*16*). Upper limits derived from the NOESY data were used as restraints for torsion angle molecular dynamics runs performed within DYANA (*17*), using its standard simulated annealing protocol. To determine the topologies of the interactions between the CPP and the DPC micelles, we measured the decrease in peak intensity in the 12 ms TOCSY spectra following addition of the micelle-integrating spin-label 5-doxylstearate, which was previously shown to be positioned in the vicinity of the phospholipid headgroups (*18*, *19*). The spin-label was added from a concentrated stock solution in methanol. Its final concentration corresponded to approximately one spin-label per micelle. Otherwise, we used our previously developed methodology as described in detail by Bader et al. (*20*, *21*).

Studies of binding of the investigated CPP to TRX were performed using a chemical shift mapping methodology. Therein, a reference $^{15}N-^{1}H$ HSQC spectrum was recorded using a 0.3 mM solution of the protein at pH 7.0, 308 K, and 100 mM MOPS buffer. Chemical shift assignments for [^{15}N]TRX were extracted from the BioMagRes database (entry 62). A separate spectrum using otherwise identical conditions was recorded after 16 equiv of the corresponding peptides had been added. Chemical shift changes after addition of the CPP for proton and nitrogen nuclei larger than 0.03 and 0.15 ppm, respectively, were considered significant.

Preparation of Calcein-Containing Large Unilamellar Vesicles (LUV). LUV were prepared by dissolving the respective phospholipids (either neutral POPC only or a mixture of 80% neutral POPC and 20% negatively charged POPG) in chloroform to ensure complete solution and mixing of the components. The lipids were dried at 37 °C in a rotary evaporator to yield a thin film and then kept under high vacuum overnight. The dry film then was redispersed in buffer [20 mM Calcein in PBS (pH 7.4) containing 1 mM EDTA for complexing of Ca^{2+} and Mg^{2+}, which could affect Calcein fluorescence], and the resulting multilamellar vesicle (MLV) dispersion was treated with five freeze−thaw cycles. LUV were obtained by extruding the sample four times through 0.4 μm and eight times through 0.1 μm Nuclepore polycarbonate membranes (*22*). A plastic syringe mounted in a centrifugation tube was filled with hydrated Sephadex G-50 gel. After being spun at 2000 rpm for 3 min, the gel column had dried and parted from the sides of the syringe. Untrapped dye was removed by the minicolumn centrifugation method (*23*). Lipid concentrations were determined by an enzymatic colorimetric test for phospholipids (MPR 2) obtained from Roche Diagnostics (Mannheim, Germany), and the LUV size was checked by photon correlation spectroscopy on a Zetasizer 3000 HSA system (Malvern, Malvern, U.K.).

Calcein Leakage Studies. Fifty microliters of a 400 μM LUV suspension was injected into 96-well plates containing 50 μL of CPP solutions at different concentrations. Calcein leakage from vesicles was monitored fluorimetrically by measuring the decrease in the extent of self-quenching (excitation at 462 nm, emission at 525 nm) after 60 min at room temperature on a Varian (Mulgrave, Australia) Cary Eclipse spectrofluorometer. The buffer blank was subtracted from all values, and the fluorescence intensity corresponding to 100% leakage was determined after the addition of Triton X-100 (*24*). Results were displayed as the percentage of maximum leakage.

Cell Culture. HeLa cells derived from a human cervix epithelial adenocarcinoma were used throughout this study. Cell culture was maintained under standard cell culture conditions at 37 °C in a humidified atmosphere containing 5% CO_2. Cells were cultured as exponentially growing subconfluent monolayers in 25 cm^2 culture flasks in Dulbecco's modified Eagle's medium supplemented with 10% heat-inactivated FCS and 1% penicillin/streptomycin. Cells were used within a range of 10 consecutive passage numbers (10−19).

Cytotoxicity. To check for cell proliferation and viability of HeLa cells after they had been treated with the CPP, we measured the overall activity of the mitochondrial dehydrogenase by an MTT assay according to the instructions of ATCC (MTT Cell Proliferation Assay Instructions) (*25*). Briefly, HeLa cells were seeded in 96-well plates at a density of 40 000 cells/cm^2. One day after seeding, cells were incubated for 2 h with the CPP at different concentrations (0.1, 1, 5, 10, 50, 100, 250, and 500 μM). Untreated cells and cells treated with methanol for 7 min were used as controls. After the CPP solution had been discarded, MTT was added for 4 h at 37 °C. After the MTT solution had been removed, the purple precipitate was dissolved over the course of 12 h by addition of a detergent (81 mL of 2-propanol, 15 mL of 20% SDS, and 4 mL of 1 M HCl). The overall activity of mitochondrial dehydrogenase in each well was measured spectrophotometrically at 570 nm using a ThermoMax microplate reader (Molecular Devices, Sunnyvale, CA).

Membrane Integrity. To check for membrane integrity, cells were seeded in 24-well plates at a density of 40 000 cells/cm^2 and used 1 day after seeding. After incubation for 2 h with the CPP at different concentrations (0, 1, 5, 10, 20, 50, and 100 μM), cells were incubated with propidium iodide (PI) (30 μg/mL in medium without serum) for 5 min, washed with PBS, and trypsinized for 7 min. PI is a cell membrane impermeable dye that develops fluorescence once bound to intracellular DNA. Cells were analyzed by FACS analysis on a FacsCalibur instrument (BectonDickinson, Franklin Lakes, NJ) within 1 h of trypsinization. A total of 8000 gated cells per sample was counted. Data were analyzed using Summit (Cytomation Inc., Fort Collins, CO).

TRX Labeling. TRX contains two cysteines that may be covalently conjugated to a fluorescent marker attached to a maleimide group. A 90 μM solution of TRX in 50 mM Tris buffer at pH 7.0 was incubated for 1 h at room temperature with a 10-fold molar excess of dithiothreitol (DTT). To remove unreacted DTT, we dialyzed against Tris buffer. Subsequently, the TRX solution was incubated together with a freshly prepared 10 μM solution of fluorescein 5-maleimide in Tris buffer overnight at 4 °C in the absence of oxygen. The reaction was quenched by adding mercaptoethanol. Fluorescently labeled TRX was separated from the unconjugated dye using a Sephadex column and used after lyophilization.

Formation of the CPP−Protein Complex. TRX or β-galactosidase was used as protein cargo, and incubated with one of the three investigated CPPs. We adapted the protocol given in the manufacturer's instructions for Chariot reagent. Briefly, TRX at a concentration of 10 μM and the respective CPP at a concentration of 200 μM were mixed together at a molar ratio of 1:20, incubated for 30 min, and diluted with serum-free medium to a final TRX concentration of 1.5 μM. Accordingly, β-galactosidase at a concentration of 1.25 μM and the CPP at a concentration of 166.5 μM were mixed together at a molar ratio of 1:130, incubated for 30 min, and diluted with serum-free medium to yield a final β-galactosidase concentration of 126 nM. CPP stock solutions were prepared in either H_2O or, when especially mentioned, 22.5% DMSO to increase the solubility as described in the manufacturer's instructions for the Chariot reagent. The final DMSO concentration was approximately 2%. No cytotoxicity was found at this concentration using a MTT assay.

Cellular Translocation of β-Galactosidase. The translocation capacity of the investigated CPP in HeLa cells was measured using β-galactosidase as the cargo. HeLa cells were seeded in 96-well plates at a density of 40 000 cells/cm^2 and used 1 day after seeding. Cells were overlaid with 100 μL of the CPP−β-galactosidase complex solution for 1 h, subsequently diluted with 200 μL of medium, and incubated for an additional 2 h at 37 °C. The translocation of β-galactosidase was monitored by cleavage of its substrate, 5-bromo-4-chloro-3-indolyl β-d-galactosidase (X-gal), which resulted in an indigo-colored precipitate in those HeLa cells which successfully internalized β-galactosidase (*26*). The β-galactosidase staining kit was used according to the manufacturer's instructions.

Cellular Translocation of TRX: Confocal Laser Scanning Microscopy (CLSM). To monitor the translocation of fluorescein-labeled TRX in HeLa cells, we used CLSM. Exponentially growing HeLa cells were seeded onto eight-well glass chamber slides at a density of 30 000 cells/cm^2 and used 1 day after seeding as exponentially growing subconfluent monolayers. For uptake, cells were incubated for 1 h with 100 μL of the CPP−TRX complex solution or 1.5 μM TRX solution alone as a control. Prior to CLSM, 200 μL of serum-containing medium was added for an additional 2 h. For the last 30 min of the incubation, Hoechst 33342 was added to a final concentration of 1 μg/mL for nuclear staining. To prepare for CLSM, cells were extensively rinsed with HBSS buffer, overlaid with HBSS buffer, and used as such without fixation. To avoid misinterpretation due to fluorescence bound to cell membranes or working materials, half of the volume was replaced with an aqueous 0.4% Trypan Blue solution (*27*−*29*). Cells were then scanned using a Zeiss (Jena, Germany) CLSM 410 inverted microscope. Image processing was performed with the software Imaris (Bitplane, Zurich, Switzerland).

Fluorescence-Activated Cell Sorting (FACS): Quantification of Translocated TRX. To quantify the translocation of TRX in HeLa cells, we applied FACS analysis. HeLa cells were seeded in 24-well plates at a density of 30 000 cells/cm^2 and used 1 day after seeding. For translocation, HeLa cells were incubated for 1 h with 200 μL of the CPP−TRX complex solution or 1.5 μM TRX solution alone as a control. Prior to FACS, 400 μL of serum-containing medium was added for an additional 2 h. In a second set of experiments, cells were preincubated prior to the experiment for 1 h with 0.1% NaN_3 and 50 mM 2-deoxy-D-glucose to deplete the level of intracellular ATP (*7*). Subsequently, cells were incubated with the Pep-1−TRX complex solution, both 0.1% NaN_3 and 50 mM 2-deoxy-D-glucose still being present. Prior to FACS analysis, 400 μL of serum-containing medium was added for an additional 2 h, again containing 0.1% NaN_3 and 50 mM 2-deoxy-D-glucose.

Cells were washed twice with PBS. Due to their positive charge, CPP−TRX complexes were expected to bind to the negatively charged cell surface, and thus were difficult to detach by a simple washing protocol. To cleave adhering CPP−TRX complexes from the cell membranes and to detach the cells from the well plates, HeLa cells were trypsinized for 7 min, as adapted from the literature (*7*, *30*). Cells were then transferred into FACS tubes and washed once with PBS prior to further analysis. To avoid misinterpretation due to extracellular CPP−TRX complexes bound to the cell membrane, half of the volume was replaced with a 0.4% Trypan Blue solution as a quencher for surface-bound fluorescence (*31*, *32*). Cells were analyzed on a FacsCalibur instrument (BectonDickinson) within 1 h of trypsinization. A total of 8000 gated cells per sample was counted. Data were analyzed using Summit (Cytomation Inc.).

RESULTS

NMR Experiments. A comparison of 120 ms NOESY data recorded on the three CPPs in the presence of DPC/SDS micelles indicated that the secondary structures of all three investigated CPPs were highly similar. Continuous stretches of sequential NOEs of amide protons [$H^N(i)-H^N(i+1)$] were observed in the segment comprising residues Trp4−Ser13. In addition, some $H^\alpha-H^N(i, i+3)$ and $H^\alpha-H^\beta(i, i+3)$ restraints typical for helically folded peptides were also observed in these stretches. The medium-range NOEs were supported by significantly lowered values for the scalar $^3J_{H^N,H^\alpha}$ couplings, which were below 5 Hz for residues 4, 7, 9, and 12. Structure calculations using distance restraints derived from the NOESY data within DYANA confirmed helical folds in these segments. As a result, the segment encompassing residues 4−13 consists of an amphipathic α-helix which is terminated by Pro15 (Figure 1). Although the helical fold of the backbone was clearly defined by the NOEs, the structure calculations revealed the presence of consistent violations of upper distance restraints. These violations were derived from multiple side chain conformers involving rotations about χ_1 of Trp residues. The latter form hydrophobic clusters in which ring stacking interactions of

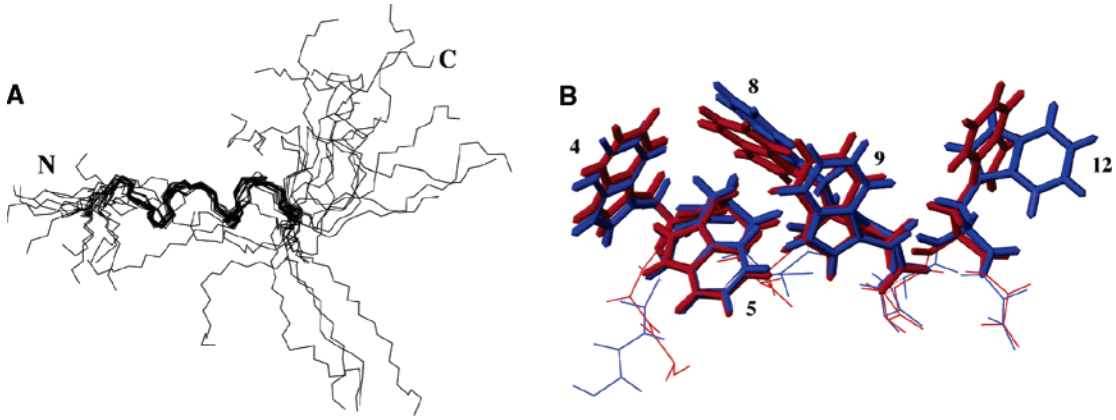

FIGURE 1: Secondary structure of PepW. (A) Backbone presentation of the superposition of 20 structures of PepW as calculated by DYANA. Backbone atoms of residues 5−13 are superimposed for the best fit. (B) Side chain conformations of Trp residues are depicted for the two major classes of conformers. Note the hydrophobic cluster formed by Trp residues 4, 5, 8, and 9 and the two side chain conformations of Trp12.

the aromatic residues occurred. Multiple well-defined conformations related to different Trp side chain rotamers occur, which were not compatible with a single structure. We conclude that upon interaction with the DPC/SDS micelles an amphipathic α-helix is formed, resulting in a hydrophobic cluster built by Trp residues (Figure 1). The NOESY experiments performed on all three peptides revealed highly similar data, indicating that the well-structured segment encompassing residues 4−13 is identical within the precision of the method. We like to emphasize at this point that we have not been able to observe intermolecular NOEs, which should have been detected in case individual pores are formed in the membrane with a lifetime sufficient to enable proteins to pass through. Such intermolecular NOEs have been observed, for example, in the case of gramicidin (*33*) or protegrin (*34*).

We used the micelle-integrating spin-label 5-doxylstearate to probe the orientation of the peptides on the micelle. It could be shown previously that the spin-label is positioned in the vicinity of the phospholipid headgroups (*18*, *19*). The relative signal attenuations due to the presence of 5-doxylstearate were plotted against the sequence for the three different peptides (Pep-1, AcPepWAmide, and PepW). In particular, the signals originating from the indole protons of Trp residues were significantly broadened, indicating that these residues primarily partition into the water−micelle interface. Signal attenuations of all three CPPs largely followed periodic patterns. Interestingly, the total extent of signal attenuations in general followed this order: PepW < AcPepWAmide < Pep-1. At present, it is unclear whether this is due to changes in membrane binding affinity or whether the data reflect differences in membrane insertion topology. However, considering that the peptides are structurally superimposable in their N-terminal structured parts and taking into account that the amounts of signal attenuation for residues on the solvent-exposed side decrease in the same order, we find increases in lifetime for the membrane-bound species are more likely to account for the observations. This indicates that binding of Pep-1 to the micelles was tighter than binding for the two other peptides, suggesting a measure for the affinity of these peptides for lipid membranes. Introduction of cysteamine at the C-terminus enhanced its membrane association, which was less pronounced for AcPepWAmide. In the case of PepW, the free C-terminus was freely diffusing in the aqueous phase. Helical periodicity was most clearly seen for PepW. Prominent signal attenuations were mainly observed for aromatic amino acids Trp4, Trp5, Trp8, Trp9, and Trp12. These findings are fully compatible with thermodynamic data for the partitioning of whole amino acids into water−membrane interfaces as measured by White and Wimely (*35*). Furthermore, the cysteamine added a new membrane anchor to the C-terminus, resulting in stronger signal attenuations along the sequence. This anchor controls the association of the peptide's C-terminus with the micelle, and thereby contributes to the overall binding (Figure 2).

By NMR, we determined the mode of binding of the CPP to a protein cargo using the chemical shift mapping methodology. As cargo, we used TRX from *E. coli*, a highly water soluble, 12 kDa cytosolic protein for which the assignment of the $^{15}N-^{1}H$ correlation map for the reduced form was published by Chandrasekhar et al. (*11*). Each of the investigated CPPs was added separately at an approximately 16-fold excess to a 0.3 mM solution of ^{15}N-labeled TRX in 100 mM MOPS buffer (pH 7.0). Figure 3A displays the secondary structure of TRX with all side chains drawn for those residues for which the ^{15}N and ^{1}H chemical shift deviations from values in the absence of the CPP exceeded 0.15 and 0.03 ppm, respectively. We calculated the electrostatic surface potential for TRX with MOLMOL, as depicted in Figure 3B. Interestingly, all major changes occurred in one contiguous region of the protein, which corresponds to the only (slightly) hydrophobic patch on the surface of this protein (Figure 3). We speculate that binding is enforced by hydrophobic contacts with the Trp cluster. Unfortunately, binding of the CPP to the cargo was very weak, preventing detection of intermolecular NOEs. Binding studies with the two other CPPs yielded highly similar results (data not shown). In all cases, hydrophobic interactions between the CPP and the cargo were fairly weak.

Effects of Peptide on Bilayer Integrity: Calcein Leakage Experiments. To check whether the investigated CPP affected the integrity of phospholipid membranes, we performed a dye leakage assay with Calcein-loaded LUV consisting of either POPC or POPC and POPG. As shown in panels A and B of Figure 4, we compared membrane-permeabilizing effects at increasing concentrations of the investigated CPP and of melittin as control in a 200 μM solution of POPC or

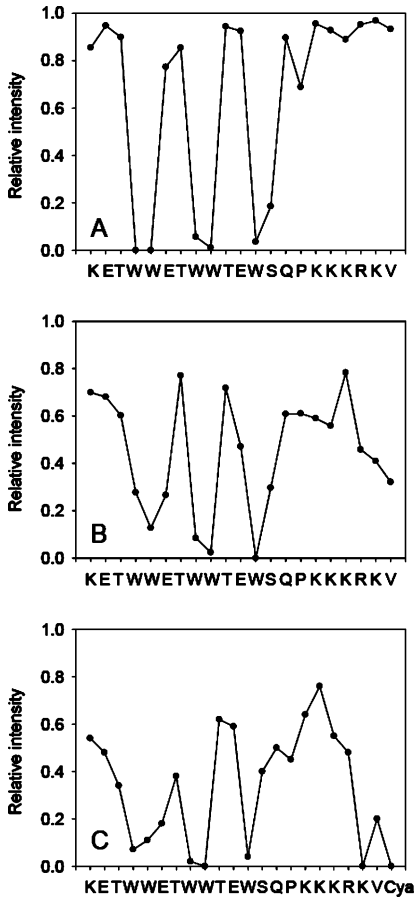

FIGURE 2: Spin-label studies. Relative signal intensities in ^{1}H TOCSY spectra of the respective CPP in DPC/SDS micelles in the presence of the spin-label 5-doxylstearic acid with respect to a reference spectrum without spin-label. The 2 mM solutions of PepW (A), AcPepWAmide (B), and Pep-1 (C) were assessed in 270 mM d_{38}-DPC/30 mM d_{25}-SDS micelles at pH 5.6.

POPC/POPG LUV at pH 7.4. In both types of LUV, melittin, a basic, amphipathic 26-amino acid peptide, for which pore formation in lipid bilayers has been demonstrated previously (*36*), led to complete Calcein leakage at a concentration as low as 1.5 μM. In contrast, PepW, AcPepWAmide, and Pep-1 did not lead to significant amounts of dye leakage in pure POPC LUV; in LUV consisting of 80% neutral POPC and 20% negatively charged POPG, at the maximal concentration of 200 μM (corresponding to a peptide-to-lipid ratio of 1.0), Pep-1, AcPepWAmide, and PepW caused extents of leakage of ~40, ~25, and ~10%, respectively.

Cytotoxicity. HeLa cells were incubated at different concentrations with the respective CPP. To check for cell viability, we measured the overall activity of mitochondrial dehydrogenase using the MTT assay. Figure 5A reveals that PepW did not compromise cell viability at a concentration of up to 500 μM. At the same concentration, AcPepWAmide caused a decrease in cell viability to 50%, and 250 μM Pep-1 to 40%, all far above the concentration of 30 μM usually used in this work for protein translocation.

Membrane Integrity. To further check for plasma membrane integrity, HeLa cells were incubated with solutions of the three investigated CPPs at different concentrations. Subsequently, cells were incubated with propidium iodide (PI). Only in the case of compromised cell membranes was PI expected to permeate the cell membrane, intercalate with nuclear DNA, and generate fluorescence. As illustrated in Figure 5B, membrane integrity after incubation with PepW or AcPepWAmide was fully preserved at any concentration up to 100 μM. In contrast, incubation with Pep-1 led to an increase in the cell membrane permeability of PI of 20% at 50 μM and of 45% at 100 μM. Clearly, none of the CPPs compromised cell membrane integrity up to 30 μM, the concentration used for protein translocation.

Translocation of TRX: Confocal Laser Scanning Microscopy (CLSM). Recently, cell fixation has been associated with artifacts that affected the mechanistic interpretation of CPP studies (*37*). Even mild fixation protocols were described to give rise to misleading conclusions about the cellular translocation of CPP (*7*, *38*). Therefore, in this work we abstained from any fixation protocols. We were also aware that routine washings with buffer alone would not reliably remove surface-bound CPP, as demonstrated in previous studies (*7*). For both CLSM and FACS, we quenched surface-bound fluorescence using Trypan blue. HeLa cells were exposed to TRX alone as a control or complexed with one of the three CPPs. For orientation, cell nuclei were stained with Hoechst 33342 and appear in blue. After incubation at 37 °C for 2 h, cellular uptake was only found in the presence of Pep-1 (Figure 6). No intracellular fluorescence was observed in cells incubated with TRX alone (Figure 6D) as a control or complexed with PepW or AcPepWAmide (Figure 6B,C).

After incubation of Pep-1 in PBS buffer for 2 h at 37 °C, we did not observe significant dimer formation as analyzed by MALDI-MS (data not shown).

Quantitative Assessment of TRX Translocation by FACS Analysis. To confirm and quantify our CLSM findings, we analyzed the cellular translocation of TRX using FACS analysis. HeLa cells were incubated with the respective CPP/TRX complex solution or with TRX alone as a control at a concentration of 1.5 μM. The relative median fluorescence of the cells after internalization is demonstrated in Figure 7. Again, Trypan blue was added as a quencher for extracellular fluorescence. Translocation of TRX only occurred in the presence of Pep-1, yielding an up to 2.5-fold increase in the relative mean fluorescence as compared to that of control cells. To summarize, FACS and CLSM data were in close agreement. After preincubation with 0.1% NaN_3 in the presence of 50 mM 2-deoxy-D-glucose, the extent of translocation of TRX into the cells was drastically reduced. The median fluorescence intensity was slightly increased compared to that of cells without incubation with fluorescently labeled TRX (Figure 8).

CPP-Mediated Delivery of β-Galactosidase in HeLa Cells. To evaluate the translocation capacity of the investigated CPP, we used β-galactosidase as cargo. The translocation of β-galactosidase was performed after mixing either Pep-1, AcPepWAmide, or PepW with β-galactosidase. An additional control experiment was performed in the absence of CPP. CPP stock solutions were diluted in water (Figure 9A−C) and in a second set of experiments in 22.5% DMSO (Figure 9E−G). The efficiency of protein translocation was determined after extensive washings followed by a β-galactosidase activity assay using X-Gal staining. Individual cells were observed by light microscopy. In the presence of Pep-1, β-galactosidase was translocated into HeLa cells, leading to vesicular distribution when CPP was diluted into H_2O

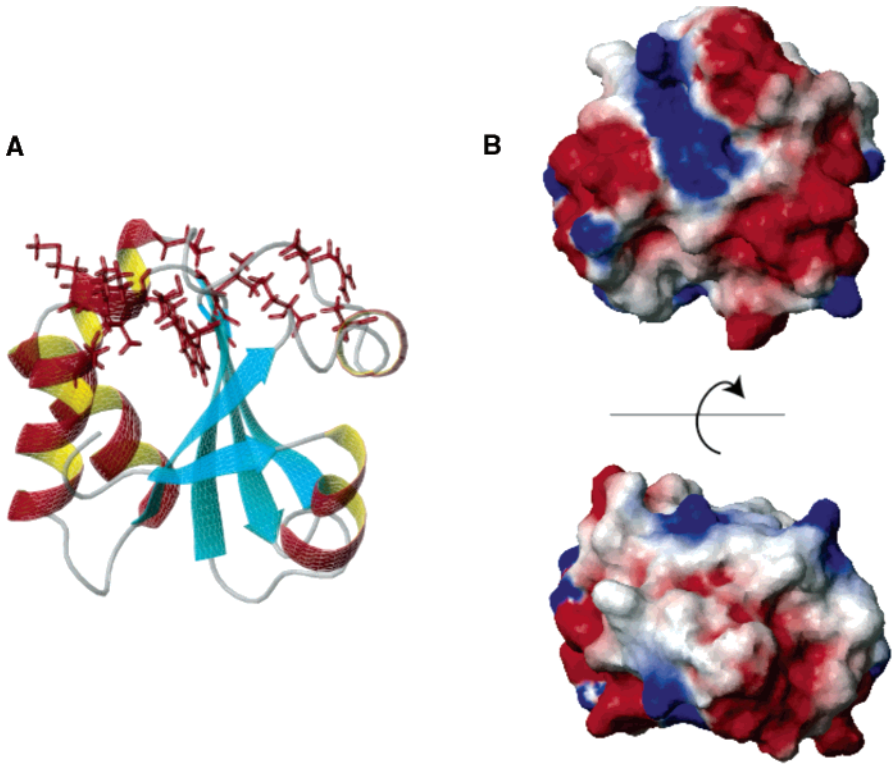

FIGURE 3: Interaction of the CPP with TRX. (A) Secondary structure of *E. coli* TRX (PDB entry 1ERT). Only side chains of residues which are significantly affected in their amide nitrogen or proton chemical shift due to the interaction with PepW were drawn. (B) Electrostatic surface potential (top) of TRX as computed in MOLMOL (*55*) (white for uncharged, red for negatively charged, and blue for positively charged) in the same spatial orientation as in the left panel, and rotated about the horizontal axis by 90° so that the face that makes contacts with PepW is turned to the front (bottom right).

(Figure 9A) versus diffuse spreading when CPP was diluted into DMSO (Figure 9E). AcPepWAmide also translocated β-galactosidase into HeLa cells, however to a lesser extent. Again, vesicular distribution was found when the peptide was diluted into H_2O (Figure 9B), and diffuse spreading was found when the peptide was diluted into DMSO (Figure 9F). PepW (Figure 9C,G) did not lead to an increase in the level of translocation as compared to the β-galactosidase control (Figure 9D,H).

DISCUSSION

Because of their potential to deliver (i) chemically conjugated or (ii) electrostatically complexed therapeutics across the plasma membrane, CPPs have recently received much attention. Less consideration has been given to (iii) hydrophobic complexes except for the previously introduced Pep-1 (*4*, *8*−*10*) also termed the Chariot peptide (Instruction manual, Chariot, ActiveMotif). Whereas its efficient translocation of various therapeutic cargoes could be demonstrated in several cell lines, its mode of action remains largely unknown. Due to its Trp-rich segment, Pep-1 is believed to form complexes with proteins through hydrophobic interactions (*8*). We focused on the influence of C- and N-terminal modifications and studied their effects on the spatial orientation of the peptide's interactions with the lipid membrane, its impact on cellular integrity and viability, and, finally, its translocation of the plasma membrane. In addition to Pep-1 with an acetylated N-terminus and with a cysteamine at the C-terminus, two modifications thereof were also investigated, namely, PepW with a free N-terminus as well as a free C-terminus, and AcPepWAmide, in which the N-terminus was acetylated and the C-terminus amidated.

The secondary structures of all investigated CPPs at pH 5.6 in phospholipid micelles were highly similar and largely helical. The main element was an α-helix comprising amino acids 4−13, terminated by Pro15. Our data for Pep-1 are in good agreement with those presented by Deshayes et al. (*4*). Therein, the authors described that the CPP adopted an α-helical conformation in water and in the presence of SDS micelles at pH 3.1 between residues 4 and 13. The N-terminal NLS sequence remained unstructured in both media (*4*). A reference CPP, penetratin, was found to adopt an α-helical conformation in the presence of SDS micelles as well as in partially negatively charged bicelles (*39*, *40*). Our spin-label study applying 5-doxylstearate demonstrated that aromatic residues Trp4, Trp5, Trp8, Trp9, and Trp12 were positioned at the water−membrane interface such that hydrophilic residues Glu2, Thr3, Glu6, Thr7, Thr10, Glu11, and Gly14 at the other face of the amphipathic helix point toward the aqueous phase. In addition, for all three investigated CPPs, the main part of the cationic nuclear localization sequence, Lys16−Lys18 and Arg19, and for AcPepWAmide and PepW also Lys20 and Val21 were exposed to the aqueous phase, whereas the C-terminal part comprising Lys20, Val21, and the cysteamine terminus of Pep-1 was found to be associated with the micelle surface. Again, as far as Pep-1 is concerned, our results were in good agreement with a recent study by Henriques et al. (*10*) and those presented by Deshayes et al. (*4*). In a fluorescence quenching study, Deshayes et al. observed a blue shift in fluorescence induced through the change in the environment of the Trp residues from a polar to a nonpolar one in the presence of phospholipid vesicles, indicating that the Trp residues become shielded from the solvent (*4*). On the basis of this outcome, the authors

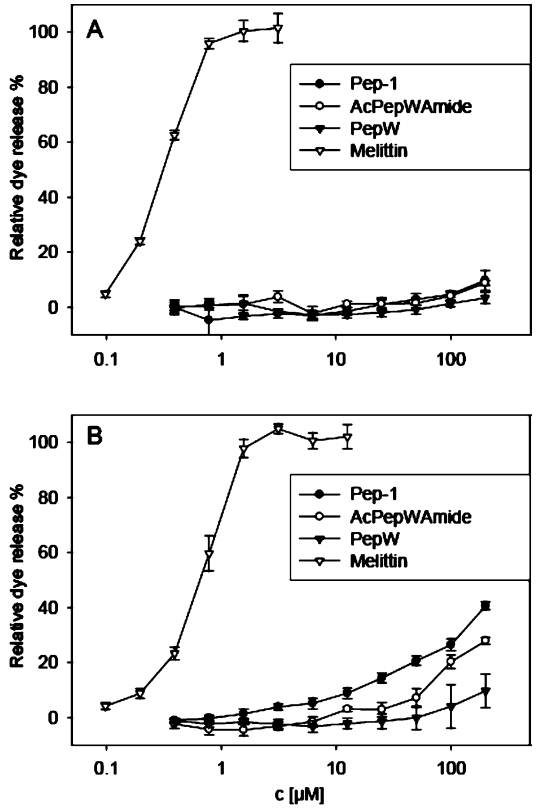

FIGURE 4: Percent leakage of the LUV-entrapped fluorescent dye Calcein as a function of CPP concentration. CPP solutions at a final concentration of up to 200 μM were added to a 400 μM POPC (A) or 320 μM POPC/80 μM POPG (B) LUV solution in PBS buffer at pH 7.4. From the increase in Calcein fluorescence, the CPP-induced leakage in percent was calculated for melittin (▽), Pep-1 (●), AcPepWAmide (○), and PepW (▼). Data were recorded after incubation for 60 min at ambient temperature (approximately 22 °C) and are represented as means ± the standard deviation (n = 3).

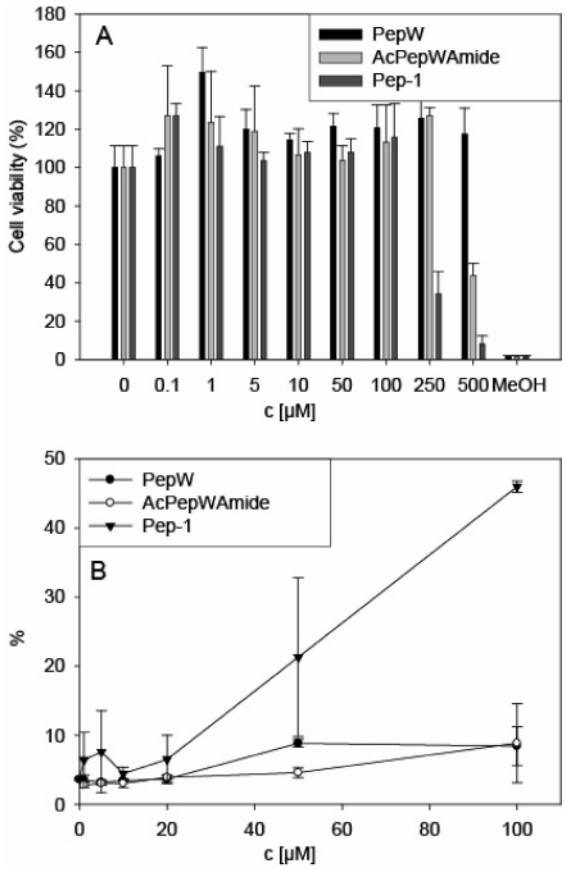

FIGURE 5: Influence on cell viability and cell membrane integrity. HeLa cells were incubated with Pep-1, AcPepWAmide, or PepW at concentrations from 0.1 to 500 μM. To check for cell viability, we measured the overall activity of mitochondrial dehydrogenase with a MTT assay. (A) PepW did not compromise cell viability up to a concentration of 500 μM, whereas AcPepWAmide reduced cell viability to 50% at a concentration of 500 μM and Pep-1 to 40% at a concentration of 250 μM. To check for membrane integrity, HeLa cells were incubated at different concentrations with the respective CPP at concentrations from 20 to 100 μM. Subsequently, cells were incubated with PI. Panel B illustrates that membrane integrity after incubation with PepW or AcPepWAmide was not compromised at any concentration up to 100 μM. In contrast, incubation with Pep-1 increased cell membrane permeability for PI to 20% at a concentration of 50 μM and to 45% at a concentration of 100 μM.

postulate that CPP−membrane interactions occur with the helical axis perpendicular to the plane of the membrane (*4*). By contrast, our spin-label data clearly reveal a three-amino acid periodicity in signal attenuations, (i) indicating that only amino acids on one distinct side of the helix were affected and (ii) establishing that the CPP associated in a parallel fashion with the surface of the micelle. This implies the hydrophobic side of the amphipathic helix binds to the interface of the lipid micelles. Previously, Lindberg et al. proposed the orientation of penetratin to be parallel to a bicelle surface. Their data were also based on data derived from paramagnetic spin-labels (*40*).

The cysteamine group in Pep-1 led to a stable anchoring of the C-terminal segment on the phospholipid micelles. The aromatic residues played a particularly important role in the interaction with the membrane, and their side chains were the most affected in the spin-label experiments. This observation is in excellent agreement with experimentally measured free energies for transferring whole amino acids from bulk solution into the membrane−water interface as determined by White and Wimley (*35*). Considering that five Trp residues are located on the hydrophobic side of the helix and that each of them contributes −1.85 kcal/mol (ΔG_{wif}) to the anchoring of the peptide in the interface, we conclude this to be the driving force for membrane anchoring. Nevertheless, hydrophobic interactions are short-range, and initial association is most likely driven by electrostatic interactions between negatively charged lipids and the basic amino acids in the NLS part of the peptides. Interestingly, such a two-step process has already been postulated using surface plasmon resonance for melittin (*41*, *42*) and for penetratin (*43*).

To study the mode by which the investigated CPPs bind to their cargo, we performed chemical shift mapping experiments using a ^{15}N-labeled hydrophilic protein, TRX from *E. coli*, as the cargo. Significant changes in the peak positions in the ^{15}N−^{1}H correlation spectrum indicated binding to the CPP, and were exclusively observed at a unique site of TRX corresponding to the only hydrophobic patch on the surface of this otherwise highly hydrophilic protein (Figure 3). Although we could not identify the interacting residues of Pep-1 directly, it seems plausible that those are the Trp residues as postulated by Morris et al. (*8*), because these represent the only hydrophobic residues in the CPP. In agreement, Deshayes et al. (*4*) described previously the

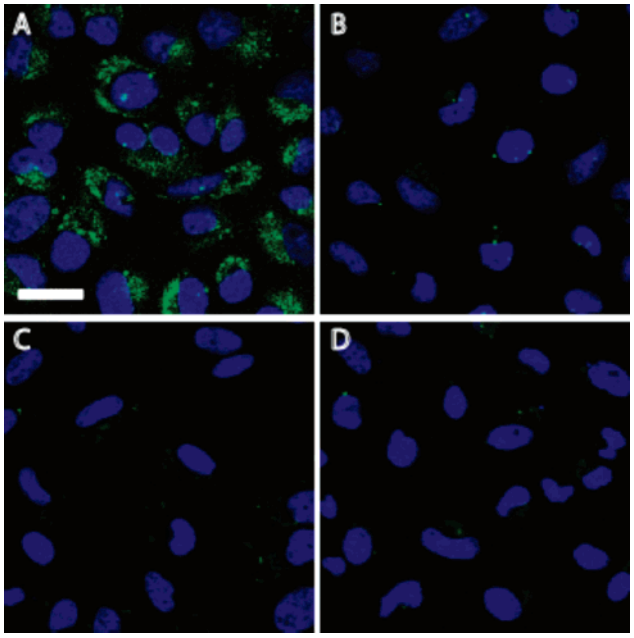

FIGURE 6: Confocal microscopy of the translocation of TRX in HeLa cells. HeLa cells were incubated for 2 h with a 1.5 μM TRX solution alone as a control (D) or complexed in a 1:20 molar ratio with (A) Pep-1, (B) AcPepWAmide, or (C) PepW. Cell nuclei (in blue) were stained for 30 min with Hoechst 33342 at a concentration of 1 μg/mL. CLSM was performed after addition of Trypan blue to quench surface-bound fluorescence.

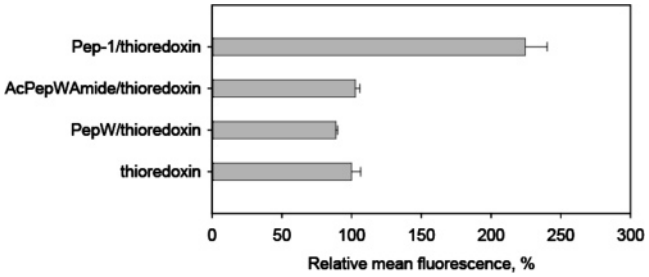

FIGURE 7: Quantification of cellular internalization of TRX in HeLa cells by FACS analysis. HeLa cells were incubated for 2 h with a 1.5 μM TRX solution alone as a control or complexed in a 1:20 molar ratio with Pep-1, AcPepWAmide, or PepW. FACS analysis was performed after addition of Trypan blue to quench surface-bound fluorescence. The internalization of TRX alone was set to 100%, and the translocation efficiencies of TRX complexed to the CPP are expressed as percentages relative to TRX alone. The results are represented as mean values $\pm$ the standard deviation ($n = 3$).

quenching of intrinsic tryptophan fluorescence of Pep-1 when complexed with a protein cargo, leading to the assumption that the tryptophans were responsible for cargo binding.

The primary result of our study was the role of the C-terminal cysteamine in greatly improving the anchoring of the peptide on the lipid membrane. The higher membrane affinity is accompanied by increased translocation efficiency for the proteins TRX and β-galactosidase in HeLa cells as shown by FACS and CLSM. We therefore conclude that the cysteamine terminus of the CPP is crucial for efficient translocation. This also indicates that the oligocationic NLS sequence is involved in the membrane reorganization process since better anchoring of the C-terminus brought its cationic residues closer to the headgroups of the lipids.

This mode of action also needs to be discussed within the context of cellular uptake. On one hand, energy-dependent cellular translocation mechanisms such as endocytosis need

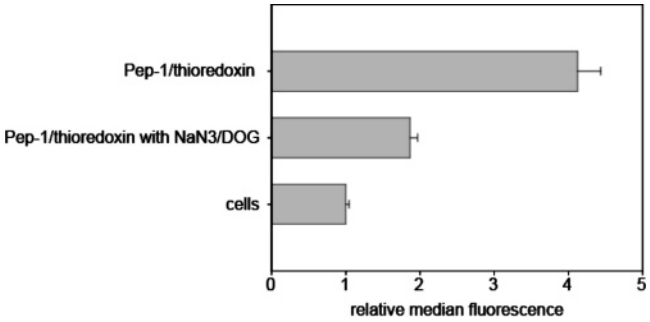

FIGURE 8: Quantification of cellular internalization of TRX complexed to Pep-1 in HeLa cells after ATP depletion. HeLa cells were incubated for 3 h with TRX complexed to Pep-1. In addition, cells were preincubated for 1 h with 0.1% NaN_3 and 50 mM 2-deoxy-D-glucose for intracellular ATP depletion. FACS analysis was performed after the addition of Trypan blue for extracellular fluorescence quenching. Results are expressed as the relative median fluorescence of TRX and are represented as median values $\pm$ the standard deviation ($n = 3$).

to be considered. Endocytosis regulates the cellular entry of small and large molecules and occurs by multiple mechanisms (*44*). Recently, a lipid raft-mediated caveolar-dependent endocytosis has been identified as the mechanism of entry for Tat fusion proteins (*45*), as well as for other CPPs (*46*). On the other hand, energy-independent mechanisms such as the pore-forming (i) barrel-stave and (ii) toroidal pore models and, to a lesser extent, (iii) carpet models and (iv) the inverted micelle model might be possible (*47*). Earlier literature described passive translocation mechanisms different from classical endocytosis for several CPPs, e.g., for penetratin (*48*) and Tat (*49*). However, more recently, data suggesting passive mechanisms were increasingly questioned on the basis of artifacts introduced through cell fixation or insufficient distinction between intracellular localization and surface-bound CPPs (*7*). Nevertheless, passive mechanisms continue to be discussed, and the exact mechanism of translocation is likely to depend on the peptide as well as on the cell line that is used. For example, melittin has been proposed to insert into the cell membrane interior and, through assembly of several monomers, form transmembrane pores (*42*) via a barrel-stave mechanism. Evidence for this mechanism was derived from dye leakage experiments. The translocation mechanism for Pep-1 has also been discussed in the literature. On the basis of electrophysiological recordings on oocytes, Deshayes et al. (*4*) proposed Pep-1 translocates passively. Translocation efficiencies at 4 and 37 °C were essentially the same which excluded a significant contribution of endocytosis as the operating mechanism (*8*). The authors have also discovered that the translocation efficiency depends on the transmembrane potential and postulated that pores are formed (*4*). In contrast, Henriques et al. exclude pore formation on the basis of their data but also find a similar dependence on the transmembrane potential (*50*, *51*). To compare the potentials of the investigated CPPs to induce membrane permeabilization, we performed a dye leakage experiment in liposomes. We observed no leakage in neutral DOPC liposomes for any of the peptides at a concentration of up to 200 μM and an only slightly but still insignificantly increased level of leakage in negatively charged liposomes. Our results for Pep-1 are in full agreement with those presented by Henriques et al. (*9*), who did not find any evidence for pores or other lytic

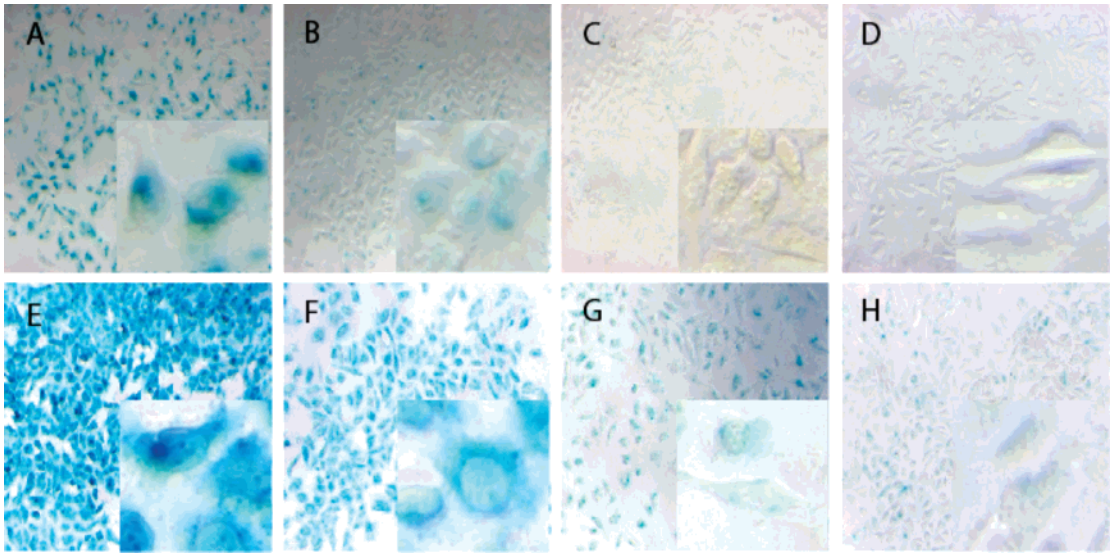

FIGURE 9: CPP-mediated delivery of β-galactosidase in HeLa cells. HeLa cells were incubated for 3 h with β-galactosidase (126 nM) alone (D and H) or when complexed at a molar ratio of 1:130 with Pep-1 (A and E), AcPepWAmide (B and F), or PepW (C and G). Protein translocation was assessed after extensive washing by following β-galactosidase activity by X-Gal staining. CPP stock solutions were diluted in H_2O (A−C) and in a second set of experiments in 22.5% DMSO (E−G).

structures. Previously, for penetratin, similar results have been found in a dye leakage study (*52*). Overall, we thus assume that the translocation mode of Pep-1 is different from the barrel-stave mechanism described for melittin. Moreover, the results from the liposome leakage study were fully supported in a membrane integrity study using PI in HeLa cells. Incubation with the CPP compromised cell membrane integrity in the following order: Pep-1 > AcPepWAmide > PepW. Importantly, leakage is only induced at concentrations much above the maximal value of 30 μM used in our cell biological studies.

Our studies of translocation efficiency in the presence of endocytose inhibitors reveal that under these conditions the efficiency for translocation is clearly reduced. However, slightly increased values compared to the control in the absence of Pep-1 also indicate that another, passive route may be employed to some minor extent. We like to emphasize that our studies were performed under conditions that are unlikely to affect membrane biophysics. This is in contrast to the usually applied decrease in temperature that will also affect the extent to which changes in membrane morphology can occur.

Further indications for an endocytic pathway for cellular uptake for Pep-1 are explained here. An early step in endocytosis is the formation of invaginations before endosome formation. It has been argued (*53*) that the phospholipid headgroups are held apart by electrostatic repulsion, and that positive charges from cationic peptides partially compensate for these charges. This allows the headgroups to approach more closely and results in the formation of a concave surface. Indeed, formation of invaginations leads to the occurrence of both convex and concave surfaces as displayed in shaded boxes B and C of Figure 10, in which the densities of the headgroups are increased or decreased as compared to the densities in nonperturbed bilayers (box A in Figure 10). Because of the oligocationic character of the NLS sequence, headgroup charges could possibly be compensated by inducing concave membrane surface curvature. The Trp residues in the N-terminal segment display a strong preference for inserting into the headgroup region and thereby pushing them further apart and induce convex curvature. Both features combined in a single peptide seem to ideally satisfy requirements for the induction of invaginations. We have recently discussed design features of CPP favoring one mode of translocation over the others (*54*) and suggested that peptides which are surface-associated and lack oligomerization interfaces favor endocytic uptake. The CPPs investigated in this study exhibit features that probably favor the inverted micelle or endocytosis mechanism over the carpet mechanism, a view that is supported by the experimental data in this work. Clearly, detailed biophysical analysis of the differences in bilayer morphology in the presence and

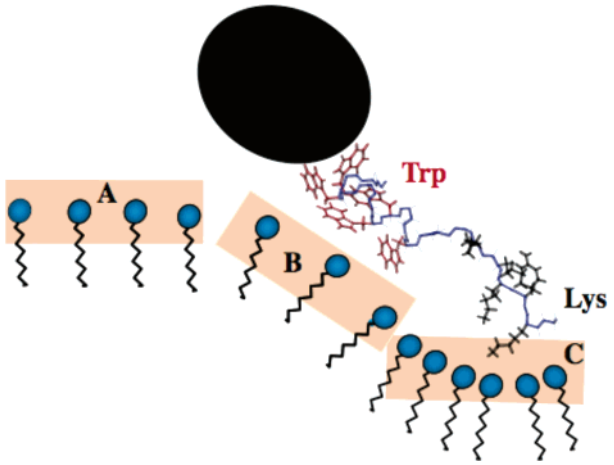

FIGURE 10: Schematic presentation of the CPP−membrane interaction. Topology of the peptide/cargo−phospholipid assembly (see the text). Only the outer leaflet of the membrane is shown. Side chains of Trp and Lys residues of the CPP are displayed and annotated in red and black, respectively. The phospholipid headgroups are held apart by electrostatic repulsion in unperturbed membranes (box A). Because of the oligocationic character of the NLS sequence, headgroup charges could possibly be compensated by inducing concave membrane surface curvature in membrane segments associated with the NLS (box C), whereas partitioning of Trp residues into the headgroup region decreases headgroup densities in those segments (box B), resulting in concave and convex curvature of the membrane surface, respectively.

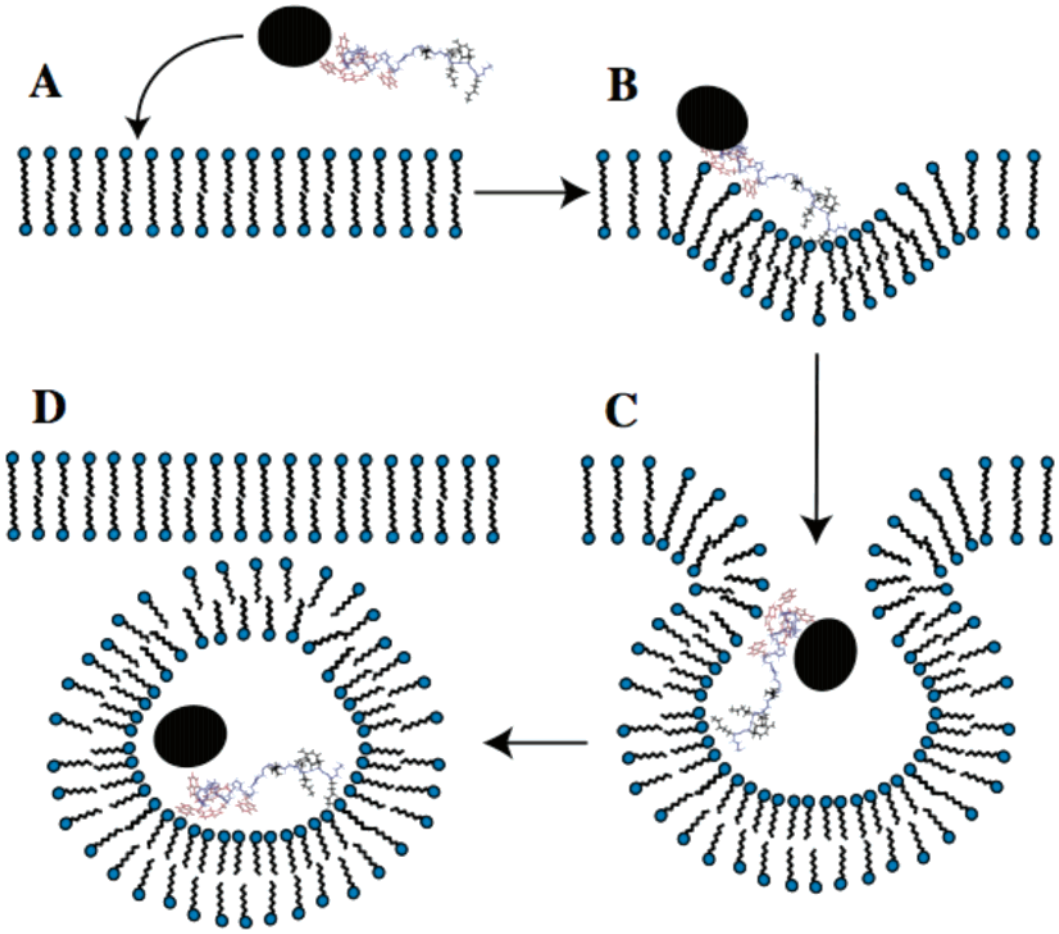

FIGURE 11: Proposed mechanism of entry of the CPPs investigated in this study. The cargo, schematically indicated as a black ball, interacts with the Trp residues of the CPP, which are also involved in anchoring the complex onto the membrane. After approaching the membrane, (A) the oligocationic NLS sequence interacts with the headgroups (B). Through partial compensation of their negative charges, a concave surface curvature might form. An invagination is built (C), which may later result in endosome formation (D).

absence of Pep-1 is required to support this speculation. A plausible scenario for the translocation process is presented in Figure 11. It proposes that the cargo is complexed via the Trp residues and that initial membrane association is promoted via electrostatic interactions involving the oligocationic C-terminal segment. From the required ratio of Pep-1 to cargo, it is clear that a number of Pep-1 molecules are likely to bind to the cargo. Once the complex approaches the membrane surface, some of them may detach from the cargo and partition into the membrane interface causing the above-described depression in the membrane while others may still be associated with the cargo via hydrophobic interactions of Pep-1 Trp residues and only associate via electrostatic interactions involving the Lys residues or the cysteamine moiety. The oligocationic NLS sequence then assumes the role of reorganizing the lipid headgroups in such a way that a concave surface curvature is induced (Figure 11B). Furthermore, N-terminal anchoring of the peptide will ensure that the bound cargo remains in the vicinity of the membrane surface so that it can be better enclosed by the now-forming vesicle (Figure 11B−D).

In our model, electrostatic interactions of the C-terminal oligolysine tail serve to partially compensate for negative headgroup charges, allowing them to approach more closely. We add at this point that this behavior thereby influences the transmembrane potential in the way that was observed by both Henriques et al. (*50*, *51*) and Heitz (*4*). However, we believe that this change is rather a result of the particular mode of interaction, and not its driving force. Moreover, it is difficult to understand how that potential itself could promote peptide translocation considering that the charges are separated by more than 20 Å. Our model proposes that translocation is initiated by formation of depressions in the membrane, and we could show that the topology of membrane association as derived from our spin-label data is consistent with our model. Although pores may be formed by the peptides transiently accounting for the electrophysiological recordings of Heitz, our studies of membrane permeation reveal that these pores are not sufficiently persistent to allow larger proteins to pass through, and we also failed to detect intermolecular NOEs proving assembly of individual molecules in the membrane. The proposed model offers a rationale for the onset of formation of membrane invaginations and is compatible both with the active endocytic mechanism and with the passive inverted micelle mode. However, our translocation studies performed under conditions of endocytose inhibition indicate that translocation mainly, but not exclusively, occurs via the active mechanism.

The proposed model is speculative in nature in that we cannot offer experimental evidence for the proposed changes in phospholipid headgroup separations at present. We hope to steer biophysical work in that direction.

ACKNOWLEDGMENT

We acknowledge Michael Herbig (ETH Zurich) for valuable discussions.

REFERENCES

1. Scheller, A., Oehlke, J., Wiesner, B., Dathe, M., Krause, E., Beyermann, M., Melzig, M., and Bienert, M. (1999) Structural requirements for cellular uptake of α-helical amphipathic peptides, *J. Pept. Sci. 5*, 185−94.
2. Drin, G., Mazel, M., Clair, P., Mathieu, D., Kaczorek, M., and Temsamani, J. (2001) Physico-chemical requirements for cellular uptake of pAntp peptide. Role of lipid-binding affinity, *Eur. J. Biochem. 268*, 1304−14.
3. Christiaens, B., Grooten, J., Reusens, M., Joliot, A., Goethals, M., Vandekerckhove, J., Prochiantz, A., and Rosseneu, M. (2004) Membrane interaction and cellular internalization of penetratin peptides, *Eur. J. Biochem. 271*, 1187−97.
4. Deshayes, S., Heitz, A., Morris, M. C., Charnet, P., Divita, G., and Heitz, F. (2004) Insight into the mechanism of internalization of the cell-penetrating carrier peptide Pep-1 through conformational analysis, *Biochemistry 43*, 1449−57.
5. Lundberg, P., and Langel, U. (2003) A brief introduction to cell-penetrating peptides, *J. Mol. Recognit. 16*, 227−33.
6. Vives, E. (2003) Cellular utake of the Tat peptide: An endocytosis mechanism following ionic interactions, *J. Mol. Recognit. 16*, 265−71.
7. Richard, J. P., Melikov, K., Vives, E., Ramos, C., Verbeure, B., Gait, M. J., Chernomordik, L. V., and Lebleu, B. (2003) Cell-penetrating peptides. A reevaluation of the mechanism of cellular uptake, *J. Biol. Chem. 278*, 585−90.
8. Morris, M. C., Depollier, J., Mery, J., Heitz, F., and Divita, G. (2001) A peptide carrier for the delivery of biologically active proteins into mammalian cells, *Nat. Biotechnol. 19*, 1173−6.
9. Henriques, S. T., and Castanho, M. A. (2004) Consequences of nonlytic membrane perturbation to the translocation of the cell penetrating peptide pep-1 in lipidic vesicles, *Biochemistry 43*, 9716−24.
10. Henriques, S. T., and Castanho, M. A. (2005) Environmental factors that enhance the action of the cell penetrating peptide pep-1: A spectroscopic study using lipidic vesicles, *Biochim. Biophys. Acta 1669*, 75−86.
11. Chandrasekhar, K., Krause, G., Holmgren, A., and Dyson, H. J. (1991) Assignment of the ^{15}N NMR spectra of reduced and oxidized *Escherichia coli* thioredoxin, *FEBS Lett. 284*, 178−83.
12. Brown, L. R., Bösch, C., and Wüthrich, K. (1981) Location and orientation relative to the micelle surface for glucagon in mixed micelles with dodecylphosphocholine: EPR and NMR studies, *Biochim. Biophys. Acta 642*, 296−312.
13. Wüthrich, K. (1986) *NMR of Proteins and Nucleic Acids*, Wiley, New York.
14. Griesinger, C., Otting, G., Wüthrich, K., and Ernst, R. R. (1988) Clean Tocsy for H-1 Spin System-Identification in Macromolecules, *J. Am. Chem. Soc. 110*, 7870−2.
15. Kumar, A., Ernst, R. R., and Wüthrich, K. (1980) A Two-Dimensional Nuclear Overhauser Enhancement (2D NOE) Experiment for the Elucidation of Complete Proton,Proton Cross-Relaxation Networks in Biological Macromolecules, *Biochem. Biophys. Res. Commun. 95*, 1−6.
16. Otting, G. (1990) Zero-Quantum Suppression in NOESY and Experiments with a z-Filter, *J. Magn. Reson. 86*, 496−508.
17. Güntert, P., Mumenthaler, C., and Wüthrich, K. (1997) Torsion Angle Dynamics for NMR Structure Calculation with the New Program Dyana, *J. Mol. Biol. 273*, 283−98.
18. Jarvet, J., Zdunek, J., Damberg, P., and Gräslund, A. (1997) Three-dimensional structure and position of porcine motilin in sodium dodecyl sulfate micelles determined by ^{1}H NMR, *Biochemistry 36*, 8153−63.
19. Papavoine, C. H., Konings, R. N., Hilbers, C. W., and Van de Ven, F. J. (1994) Location of the M13 coat protein in sodium dodecyl sulfate micelles as determined by NMR, *Biochemistry 33*, 12990−7.
20. Bader, R., Bettio, A., Beck-Sickinger, A. G., and Zerbe, O. (2001) Structure and dynamics of micelle-bound neuropeptide Y: Comparison with unligated NPY and implications for receptor selection, *J. Mol. Biol. 305*, 307−29.
21. Bader, R., Lerch, M., and Zerbe, O. (2002) in *BioNMR in Drug Research* (Zerbe, O., Ed.) pp 95−120, Wiley-VCH, Weinheim, Germany.
22. Mayer, L. D., Hope, M. J., and Cullis, P. R. (1986) Vesicles of variable sizes produced by a rapid extrusion procedure, *Biochim. Biophys. Acta 858*, 161−8.
23. New, R. B. C. (1990) *Liposomes, A Practical Approach*, Oxford University Press, New York.
24. Dathe, M., Schumann, M., Wieprecht, T., Winkler, A., Beyermann, M., Krause, E., Matsuzaki, K., Murase, O., and Bienert, M. (1996) Peptide helicity and membrane surface charge modulate the balance of electrostatic and hydrophobic interactions with lipid bilayers and biological membranes, *Biochemistry 35*, 12612−22.
25. Lobner, D. (2000) Comparison of the LDH and MTT assays for quantifying cell death: Validity for neuronal apoptosis? *J. Neurosci. Methods 96*, 147−52.
26. Singh, D., Bisland, S. K., Kawamura, K., and Gariepy, J. (1999) Peptide-based intracellular shuttle able to facilitate gene transfer in mammalian cells, *Bioconjugate Chem. 10*, 745−54.
27. Sahlin, S., Hed, J., and Rundquist, I. (1983) Differentiation between Attached and Ingested Immune-Complexes by a Fluorescence Quenching Cytofluorometric Assay, *J. Immunol. Methods 60*, 115−24.
28. Ma, Z. S., and Lim, L. Y. (2003) Uptake of chitosan and associated insulin in Caco-2 cell monolayers: A comparison between chitosan molecules and chitosan nanoparticles, *Pharm. Res. 20*, 1812−9.
29. Wan, C. P., Park, C. S., and Lau, B. H. S. (1993) A Rapid and Simple Microfluorometric Phagocytosis Assay, *J. Immunol. Methods 162*, 1−7.
30. Tseng, W. C., Purvis, N. B., Haselton, F. R., and Giorgio, T. D. (1996) Cationic liposomal delivery of plasmid to endothelial cells measured by quantitative flow cytometry, *Biotechnol. Bioeng. 50*, 548−54.
31. Hed, J., Hallden, G., Johansson, S. G., and Larsson, P. (1987) The use of fluorescence quenching in flow cytofluorometry to measure the attachment and ingestion phases in phagocytosis in peripheral blood without prior cell separation, *J. Immunol. Methods 101*, 119−25.
32. Innes, N. P., and Ogden, G. R. (1999) A technique for the study of endocytosis in human oral epithelial cells, *Arch. Oral Biol. 44*, 519−23.
33. Arseniev, A. S., Barsukov, I. L., Bystrov, V. F., Lomize, A. L., and Ovchinnikov, Yu. A. (1985) ^{1}H NMR study of gramicidin A transmembrane ion channel. Head-to-head right-handed, single-stranded helices, *FEBS Lett. 186*, 168−74.
34. Roumestand, C., Louis, V., Aumelas, A., Grassy, G., Calas, B., and Chavanieu, A. (1998) Oligomerization of protegrin-1 in the presence of DPC micelles. A proton high-resolution NMR study, *FEBS Lett. 421*, 263−7.
35. White, S. H., and Wimley, W. C. (1998) Hydrophobic interactions of peptides with membrane interfaces, *Biochim. Biophys. Acta 1376*, 339−52.
36. Matsuzaki, K., Sugishita, K., and Miyajima, K. (1999) Interactions of an antimicrobial peptide, magainin 2, with lipopolysaccharide-containing liposomes as a model for outer membranes of Gram-negative bacteria, *FEBS Lett. 449*, 221−4.
37. Lundberg, M., and Johansson, M. (2001) Is VP22 nuclear homing an artifact? *Nat. Biotechnol. 19*, 713−4.
38. Drin, G., Cottin, S., Blanc, E., Rees, A. R., and Temsamani, J. (2003) Studies on the internalisation mechanism of cationic cell-penetrating peptides, *J. Biol. Chem. 278*, 31192−201.
39. Lindberg, M., and Gräslund, A. (2001) The position of the cell penetrating peptide penetratin in SDS micelles determined by NMR, *FEBS Lett. 497*, 39−44.
40. Lindberg, M., Biverstahl, H., Gräslund, A., and Mäler, L. (2003) Structure and positioning comparison of two variants of penetratin in two different membrane mimicking systems by NMR, *Eur. J. Biochem. 270*, 3055−63.
41. Lee, T. H., Mozsolits, H., and Aguilar, M. I. (2001) Measurement of the affinity of melittin for zwitterionic and anionic membranes using immobilized lipid biosensors, *J. Pept. Res. 58*, 464−76.
42. Mozsolits, H., Wirth, H. J., Werkmeister, J., and Aguilar, M. I. (2001) Analysis of antimicrobial peptide interactions with hybrid bilayer membrane systems using surface plasmon resonance, *Biochim. Biophys. Acta 1512*, 64−76.
43. Dom, G., Shaw-Jackson, C., Matis, C., Bouffioux, O., Picard, J. J., Prochiantz, A., Mingeot-Leclercq, M. P., Brasseur, R., and Rezsohazy, R. (2003) Cellular uptake of Antennapedia Penetratin

peptides is a two-step process in which phase transfer precedes a tryptophan-dependent translocation, *Nucleic Acids Res. 31*, 556−61.
44. Conner, S. D., and Schmid, S. L. (2003) Regulated portals of entry into the cell, *Nature 422*, 37−44.
45. Fittipaldi, A., Ferrari, A., Zoppe, M., Arcangeli, C., Pellegrini, V., Beltram, F., and Giacca, M. (2003) Cell membrane lipid rafts mediate caveolar endocytosis of HIV-1 Tat fusion proteins, *J. Biol. Chem. 278*, 34141−9.
46. Foerg, C., Ziegler, U., Fernandez-Carneado, J., Giralt, E., Rennert, R., Beck-Sickinger, A. G., and Merkle, H. P. (2005) Decoding the Entry of Two Novel Cell-Penetrating Peptides in HeLa Cells: Lipid Raft-Mediated Endocytosis and Endosomal Escape, *Biochemistry 44*, 72−81.
47. Magzoub, M., and Gräslund, A. (2004) Cell-penetrating peptides: Small from inception to application, *Q. Rev. Biophys. 37*, 147−95.
48. Derossi, D., Joliot, A. H., Chassaing, G., and Prochiantz, A. (1994) The third helix of the Antennapedia homeodomain translocates through biological membranes, *J. Biol. Chem. 269*, 10444−50.
49. Vives, E., Brodin, P., and Lebleu, B. (1997) A truncated HIV-1 Tat protein basic domain rapidly translocates through the plasma membrane and accumulates in the cell nucleus, *J. Biol. Chem. 272*, 16010−7.
50. Henriques, S. T., Costa, J., and Castanho, M. A. (2005) Re-evaluating the role of strongly charged sequences in amphipathic cell-penetrating peptides: A fluorescence study using Pep-1, *FEBS Lett. 579*, 4498−502.
51. Henriques, S. T., Costa, J., and Castanho, M. A. (2005) Translocation of β-galactosidase mediated by the cell-penetrating peptide pep-1 into lipid vesicles and human HeLa cells is driven by membrane electrostatic potential, *Biochemistry 44*, 10189−98.
52. Drin, G., Demene, H., Temsamani, J., and Brasseur, R. (2001) Translocation of the pAntp peptide and its amphipathic analogue AP-2AL, *Biochemistry 40*, 1824−34.
53. Kirk, G. L., Gruner, S. M., and Stein, D. L. (1984) A thermodynamic model of the lamellar to inverse hexangonal phase transition of lipid-membrane water systems, *Biochemistry 23*, 1093−102.
54. Herbig, M. E., Weller, K., Krauss, U., Beck-Sickinger A., Merkle, H. P., and Zerbe, O. (2005) Membrane surface associated helices promote lipid interactions and cellular uptake of human calcitonin-derived cell penetrating peptides, *Biophys. J.* (in press).
55. Koradi, R., Billeter, M., and Wüthrich, K. (1996) MOLMOL: A program for display and analysis of macromolecular structures, *J. Mol. Graphics 14*, 51−5, 29−32.

BI051535D